

Review

1D Titanium Dioxide: Achievements in Chemical Sensing

Navpreet Kaur , Mandeep Singh , Abderrahim Moumen, Giorgio Duina and Elisabetta Comini * 

SENSOR Laboratory, Department of Information Engineering, University of Brescia, Via Valotti 9, 25133 Brescia, Italy; n.kaur001@unibs.it (N.K.); mandeep.singh@unibs.it (M.S.); a.moumen@unibs.it (A.M.); giorgio.duina@unibs.it (G.D.)

* Correspondence: elisabetta.comini@unibs.it; Tel.: +39-030-3715877

Received: 28 May 2020; Accepted: 30 June 2020; Published: 3 July 2020



Abstract: For the last two decades, titanium dioxide (TiO₂) has received wide attention in several areas such as in medicine, sensor technology and solar cell industries. TiO₂-based gas sensors have attracted significant attention in past decades due to their excellent physical/chemical properties, low cost and high abundance on Earth. In recent years, more and more efforts have been invested for the further improvement in sensing properties of TiO₂ by implementing new strategies such as growth of TiO₂ in different morphologies. Indeed, in the last five to seven years, 1D nanostructures and heterostructures of TiO₂ have been synthesized using different growth techniques and integrated in chemical/gas sensing. Thus, in this review article, we briefly summarize the most important contributions by different researchers within the last five to seven years in fabrication of 1D nanostructures of TiO₂-based chemical/gas sensors and the different strategies applied for the improvements of their performances. Moreover, the crystal structure of TiO₂, different fabrication techniques used for the growth of TiO₂-based 1D nanostructures, their chemical sensing mechanism and sensing performances towards reducing and oxidizing gases have been discussed in detail.

Keywords: titanium dioxide; nanostructures; heterostructures; chemical sensing

1. Introduction

With the worldwide industrial and technological growth, there is a continuous demand for portable, low-cost and efficient sensing devices that can be used for various purposes such as environmental monitoring and health care. Due to this, researchers have made continuous efforts to find new materials or to grow existing materials in different forms such as thin films and nanostructures. In the field of chemical sensors, nanostructured metal oxides (MOX) are the most versatile and widely studied active sensing materials due to their unique physical/chemical properties [1]. Their wide band gap, along with the exceptional electrical properties, makes MOXs among the leading candidate for transparent electronic devices [2]. Indeed, tin oxide (SnO₂) in different nanostructures forms such as nanowires [3,4], nanobelt [5,6] and nanorods [7,8] is the most widely investigated material in the field of chemical/gas sensing.

Among the different nanostructures' forms, one-dimensional (1D) nanostructures such as nanowires exhibit unique properties such as high surface to volume ratio, high crystallinity and controlled electrical properties which make them interesting for chemical sensing applications [3,9–12]. Because there is no requirement of preliminary gas diffusion to the surface, 1D MOX gas sensors showed faster response dynamics. Moreover, the self-heating phenomenon of nanowires can be used to reduce the power consumption of temperature-driven devices such as conductometric gas

sensors, as nanowires attain high temperature when they undergo electrical resistance measurements, even when low electrical power has been used during the measurements [1,13].

Recently, MOXs such as zinc oxide (ZnO) [14], nickel oxide (NiO) [15], titanium dioxide (TiO₂) [12] and tungsten oxide (WO₃) [11] have been grown in the form of 1D nanostructures and were used for the detection of different gas analytes. Among these MOXs, TiO₂ is one of the most versatile ones and is widely used for many different applications, including photocatalysis [16], sensors [17,18] and photovoltaic applications [19]. In particular, due to its exceptional physical/chemical properties, TiO₂ was extensively used for different sensing applications such as chemical/gas sensors [20,21], biosensors [17,22] and chemical oxygen demand (COD) [23,24] sensors [25]. It typically exhibits n-type conductivity and, in nanostructured form, is chemically stable, biocompatible, biodegradable and inexpensive [25]. It exhibits three different crystal structures—namely, anatase, rutile and brookite, each of them possessing unique structural, electrical and optical properties [26]. Rutile TiO₂ is widely used as a pigment, opacifier, isolator, and in switches, etc. due to its light-scattering ability, high refractive index and ultraviolet (UV) absorptivity, while anatase TiO₂ is preferred for photovoltaic and photocatalytic applications [27]. On the other hand, brookite is the rarest occurring phase of TiO₂, which is formed under a particular set of conditions. Due to this, brookite TiO₂ has been very rarely investigated materials and its applications in fields such as photovoltaic applications [28] and lithium ion batteries [29] were recently discovered.

In this review article, recent achievements of 1D TiO₂ chemical/gas sensors will be presented. Specifically, crystal structure of TiO₂, MOX gas sensing mechanism and techniques used to grow 1D TiO₂ nanostructures will be discussed in detail. In order to describe the recent achievements of 1D TiO₂ chemical sensors, literature reported over the span of the last five to seven years will be presented.

2. Crystal Structure of TiO₂

The structural properties of the active sensing material in a gas sensor (either in bulk, thin films or nanostructures form) are among the most important characteristics, as they influence the electrical, optical and mechanical behavior of the material. In particular, the surface structure and defectivity/stoichiometry of metal oxides has a great influence on local surface chemistry [26] and, consequently, they affect their performances as active sensing materials decisively. It is therefore important to understand the crystal structure of a chemo-resistive MOX to be used in a sensing device and to study how its structural properties may change as a function of the growth parameters (such as temperature). Hence, in this section, we will discuss the crystal structure of TiO₂.

TiO₂ exists in nature as well-known minerals rutile (tetragonal), anatase (tetragonal) and brookite (orthorhombic) [30]. In addition to these forms, two high-pressure forms of TiO₂ also exist, i.e., a monoclinic baddeleyite-like form and an orthorhombic α -PbO₂-like form, which were found at Ries Crater in Bavaria [31]. Indeed, rutile is the most thermodynamically stable polymorph of TiO₂.

Figure 1 shows the crystal structures of the TiO₂ anatase, rutile and brookite phases [32], and their corresponding crystal data are shown in Table 1 [26,33,34]. It should be noted that, due to the rare existence of brookite phase, the anatase and rutile forms of TiO₂ are the most exploited in real applications.

All the crystal structures of TiO₂ are made up of distorted octahedra, each one representing a TiO₆ unit, where Ti⁴⁺ is at the center of the unit and coordinates six O²⁻ ions. The way in which octahedra assemble to form the TiO₆ chain is different for each crystal structure. Anatase and rutile crystal structures are assembled by connecting the octahedra by their vertices and edges, respectively, while in brookite, both vertices and edges are connected [34].

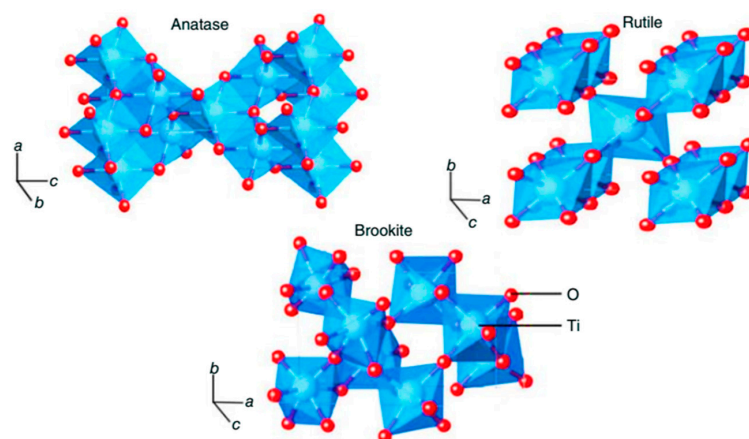


Figure 1. Different crystal structures of titanium dioxide (anatase, rutile and brookite). Reprinted with permission from ref. [32] WILEY Copyright 2019.

Table 1. Crystal structure data of the three main polymorphs of TiO₂ [26,33,34].

Crystal Structure	System	Space Group	Lattice Constants (nm)			
			a	b	c	c/a
Rutile	Tetragonal	D_{4h}^{14} —P4 ₂ /mmm	0.4584	-	0.2953	0.644
Anatase	Tetragonal	D_{4h}^{14} —I4 ₁ /amd	0.3733	-	0.937	2.51
Brookite	Rhombohedral	D_{2h}^{15} —Pbca	0.5436	0.9166	-	0.944

At room temperature, the anatase phase is kinetically stable and does not undergo any phase transformation. Nevertheless, it can be converted into rutile via heating at high temperature [26]. The anatase-to-rutile thermally-induced transition in bulk TiO₂ starts occurring at temperature $T > 600$ °C. M.N. Asiah et al. [12] have studied the phase transformation of TiO₂ nanowires grown by means of a hydrothermal method. They found that, up to 500 °C, the nanowires (anatase phase) retained their morphology, and they started to change into smaller particles at around 600 °C. At 900 °C, the complete transformation from anatase to rutile phase occurred and the nanowires' shapes changed to rod-like structures. Figure 2 shows the SEM images on TiO₂ nanowires corresponding to the different temperatures [8].

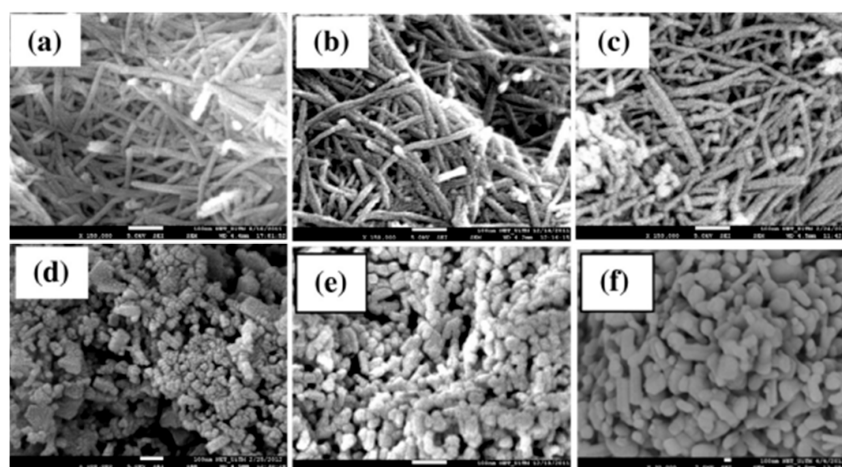


Figure 2. FESEM images of the as-prepared nanowires (a) and nanowires annealed at (b) 400 °C, (c) 500 °C, (d) 600 °C, (e) 700 °C and (f) 900 °C. Reprinted with permission from Ref. [12] Elsevier Copyright 2013.

Moreover, it was also found that the surface defects and lattice concentration play a crucial role during the phase transformation [34]. Specifically, the surface defects acted as nucleation sites and the rate of rutile transformation increased with an increase in surface defects. The removal of oxygen ions from TiO_2 lattice (i.e., the formation of oxygen vacancies) also accelerated the rutile phase formation.

3. Synthesis of TiO_2 -Based 1D Nanostructures

This thematic study acquaints the fabrication techniques commonly used for the synthesis of TiO_2 nanostructures. In the past decade, diverse fabrication methods, including chemical vapor deposition (CVD) [35], atomic layer deposition (ALD) [36], electrochemical deposition [37], hydrothermal methods [38], sol-gel [39] and electrospinning [40] have been successfully used for the preparation of high-quality TiO_2 based nanostructures. The goal of this section is to elucidate the fabrication methods most commonly employed in the last five to seven years.

3.1. Hydrothermal Synthesis

Hydrothermal synthesis is one of the most widely used techniques for the growth of TiO_2 nanostructures. This synthesis process is normally performed in steel autoclaves with or without Teflon liners under controlled pressure and temperature in an aqueous solution. All the experimental parameters involved in a hydrothermal process (e.g., annealing treatment, specific titanium precursor and process duration) influence the nanostructure growth. However, the nature of aqueous solution (acid/alkali concentration) has a major role in the structure morphology and crystallinity. B. Zaho et al. [38] reported that five different Titania/Titanate phases could be generated by employing a proper composition of acid (HCl) and alkali. High HCl concentration (6 M) lead to the formation of rutile nanorods, while monoclinic trititanate $\text{Na}_2\text{Ti}_3\text{O}_7$ nanoribbons were formed at high NaOH concentration (10 M), as shown in Figure 3. These transitions have been explained by the Ostwald's ripening mechanism [41].

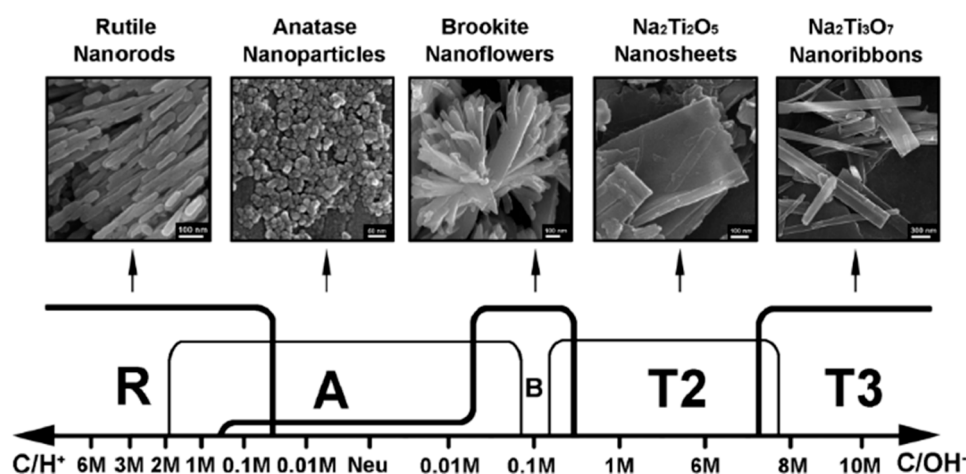


Figure 3. The effect of acid/alkali concentration. Rutile TiO_2 , anatase TiO_2 , brookite TiO_2 , dititanate $\text{Na}_2\text{Ti}_2\text{O}_5$ and trititanate $\text{Na}_2\text{Ti}_3\text{O}_7$ are represented by “R, A, B, T2 and T3”, respectively. Reprinted with permission from Ref. [38] RSC Copyright 2012.

On the other hand, recently, many reports have been published on using hydrothermal synthesis for the growth of TiO_2 nanowires (NWs) and nanorods (NRs) of rutile and anatase phase [42–44]. Generally speaking, typical processes to produce TiO_2 nanorod arrays inside a steel autoclave involve a Ti precursor, HCl solution and deionized water, heated up at 150 °C for at least 9 h, followed by thermal annealing [42,43]. Another interesting work by G. Zaho et al. [44] reports about the growth of bridge-like structures of TiO_2 NRs using isopropyl titanate as a precursor (Figure 4). Additionally,

using Ti foil or TiO₂ nanoparticles in appropriate concentrations of NaOH/ HCl and deionized water leads to successful growth of anatase TiO₂ nanowires and nanotubes [45,46].

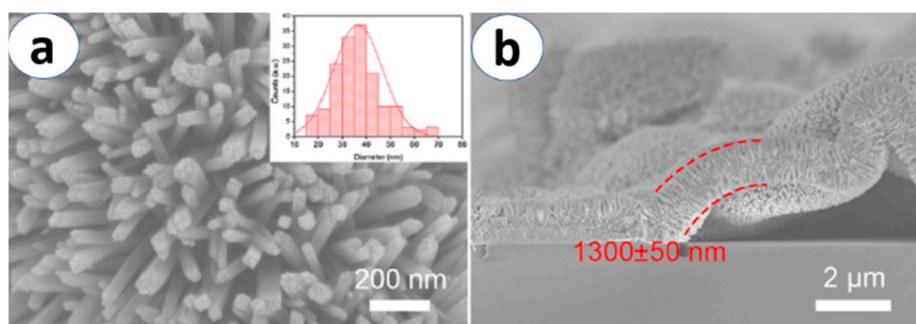


Figure 4. SEM images of TiO₂ nanorods prepared using the hydrothermal method. (a) Top and (b) cross-sectional views of the nanorods. Reprinted with permission from Ref. [44] ACS Copyright 2020.

3.2. Electrochemical Anodization

Electrochemical anodization is an efficient method for the growth of well-aligned and highly ordered nanotubes (NTs). In a typical process, the NTs are produced at room temperature using a current generator in a cell consisting of an electrolyte and two electrodes—titanium (anode) and platinum (cathode). From the reported literature, it has been seen that the water-based ethylene glycol and ammonium fluoride aqueous electrolytes are the most commonly used for anodization of titanium to fabricate TiO₂ NTs [47–50].

Generally, for the production of highly ordered NTs, an annealing treatment is required after the anodization. Different parameters such as voltage applied, anodization time and type of electrolyte solution are the major factors that influence the growth process [31,51,52]. It has been reported that highly uniform and longer NTs can be achieved when using high voltage, while the anodization time can majorly affect the length of NTs, but not their morphology [53,54]. Reports by B. Munirathinam et al. [53] and H. Sopha et al. [51] stated that the nature and the age of the electrolyte have major effects on the morphology and aspect ratio of NTs, as shown in Figure 5. This technique is usually carried out at room temperature, and it opens up great possibilities in the use of different substrates for an ultimate objective of fabricating new generation devices.

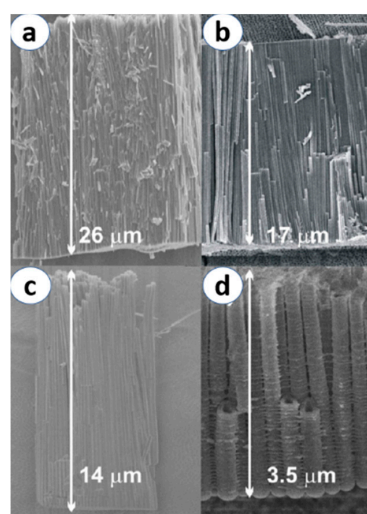


Figure 5. Cross-sectional images of TiO₂ nanotubes synthesized by applying 60 V for 6 h using different electrolyte ages: (a) fresh electrolyte, (b) 6 h, (c) 25 h and (d) 50 h. Reprinted with permission from Ref. [51] Copyright 2015 Elsevier.

3.3. Electrospinning

In comparison to the above-mentioned growth techniques, electrospinning is one of the most simple and flexible methods to synthesize the large-scale 1D TiO₂ nanostructures, especially long nanofibers of TiO₂. Figure 6 shows a schematic diagram of the electrospinning equipment [55]. In this method, a liquid precursor solution is injected through a spinneret under an applied electric field and spin force to create fibrous structures. A post-annealing treatment is commonly needed to remove the solvent and to solidify the nanofibers. In recent years, electrospinning technique has been used not only to fabricate pristine nanostructures of TiO₂, but also the composite [56–60].

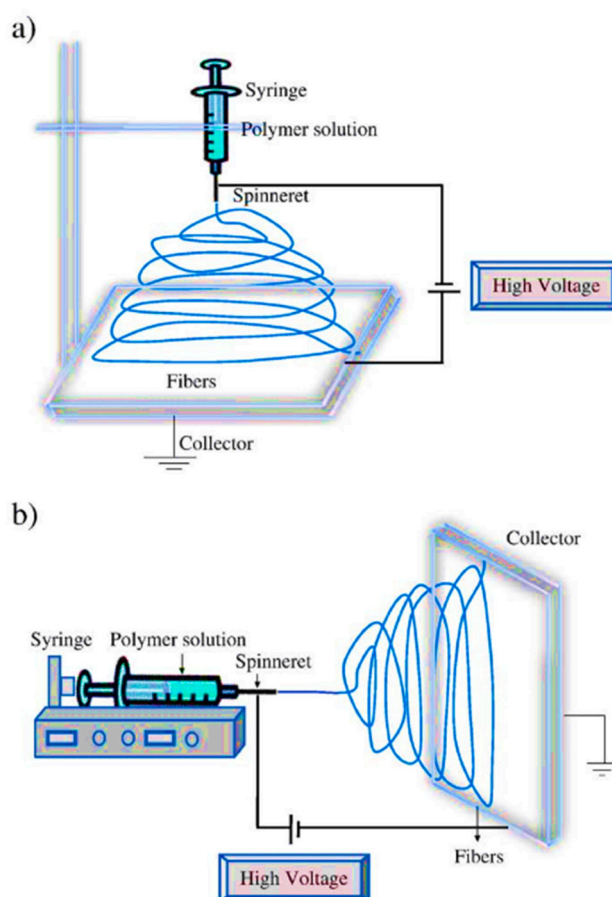


Figure 6. Schematic diagram of the electrospinning equipment (a) vertical and (b) horizontal setups. Reprinted with permission from Ref. [55], Copyright 2013 Elsevier.

In a recent report by M. Zhou et al. [56], the authors synthesized TiO₂ nanowires of different phases using the typical electrospinning method. Authors studied the effect of calcination temperature after the electrospinning of the nanowires at 500 °C, 600 °C, 700 °C and 800 °C for 2 h in air (shown in Figure 7). It was discovered that by increasing the annealing temperature, the grain size and pore size increase as well, and a phase transition from rutile to anatase TiO₂ occurs, while the band gap decreases.

Another interesting report, authored by S. Wang et al. [57], reported the fabrication of TiO₂ nanowires with two different methods, namely, an ethylene glycol-mediated method and a high-voltage electrospinning method. The nanowires synthesized via the solution method were found to be relatively uniform, having an average diameter around 550 ± 90 nm and a length of 26 ± 5 μ m. On the other hand, nanowires grown with the electrospinning method were found to be much smaller, exhibiting an average diameter of 70 ± 5 nm and a length of 12 ± 5.5 μ m. In 2017, F. Li et al. [59] presented the coaxial electrospinning method using two precursors to fabricate the core-shell nanostructures of TiO₂/SnO₂.

The structural characterizations showed two mixed phases of tetragonal SnO₂ and rutile TiO₂ with no other impurity diffraction peaks evidenced by X-ray diffraction analysis.

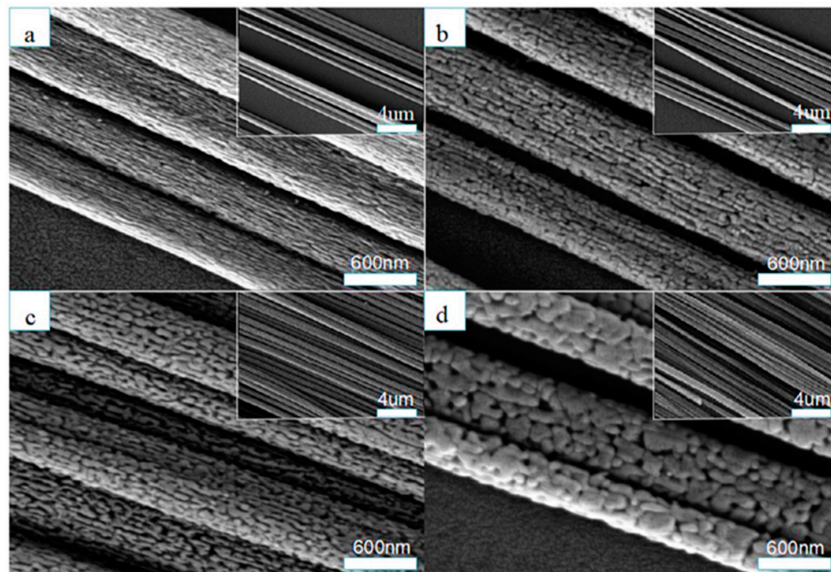


Figure 7. SEM images of aligned TiO₂ NWs calcinated at different temperatures: (a) 500 °C, (b) 600 °C, (c) 700 °C and (d) 800 °C. Reprinted with permission from Ref. [56], Copyright 2019 Elsevier.

Moreover, besides the above-mentioned growth process for TiO₂ nanostructures, the other least used techniques within the last five year were thermal oxidation [61], acid vapor deposition (AVO) [62] and the vapor phase growth process [63].

Finally, the various reports published in the last five years on the growth of TiO₂ nanostructures and its composites have been collected in Table 2, while in Table 3, some the major advantages and disadvantages related to these techniques have been presented.

Table 2. Summarization of different materials, parameters, crystal phase involved in the growth process of TiO₂ nanostructures and its composites for different fabrication techniques.

Hydrothermal					
Metal Oxide	Materials/Parameters	Nanostructure Type	Sized	Crystalline Phases	Ref./Year
TiO ₂	Titanium butoxide, hydrochloric acid and deionized water/ Temp. = 150 °C Time = 18 h	Nanorods	length = 5 μm diameter = 100 nm	rutile	[42]/2015
TiO ₂	Isopropyl titanate, hydrochloric acid Temp. = 150 °C Time = 3, 6, and 9 h	Nanorods	length = 4200 nm diameter = 120 nm	rutile	[44]/2020
TiO ₂	TiCl ₄ , HCl and deionized water Temp. = 180 °C Time = 3 h	Nanorods	diameter = 21.20 nm length = NA	anatase/rutile mixed phases	[64]/2017
TiO ₂ -Ag ₂ O	TiCl ₄ , deionized water Temp. = 180 °C Time = 3 h	Composite Nanorods	diameter = 100 nm	rutile	[65]/2019
Bi-TiO ₂	[Bi(NO ₃) ₃ ·5H ₂ O] and TiO ₂ nanoparticles with NaOH and water. Temp. = 140 °C Time = 24 h	Nanotubes	diameter = NA length = NA	anatase	[46]/2017
TiO ₂	Titanium (IV) isopropoxide, NaOH and ethanol. Temp. = 150 °C Time = 20 h	Nanowires	length = 1825 nm diameter = 30–50 nm	anatase	[66]/(2018)

Table 2. Cont.

Hydrothermal					
Metal Oxide	Materials/Parameters	Nanostructure Type	Sized	Crystalline Phases	Ref./Year
Electrochemical Anodization					
TiO ₂	Ti foil in ethylene glycol, acide phosphorique (H ₃ PO ₄) and hydrofluoric acid HF. Anodization = 120 V Temp. = RT Time = 2 h	Nanotubes	length = 20 µm diameter = 80–120 nm	anatase/rutile mixed phases	[67]/2015
7TiO ₂	Ti foil in ethylene glycol, deionized water and ammonium fluoride (NH ₄ F) Anodization = 1 From 0 V to 60 V Time = 4 h Temp. = RT	Nanotubes	length = 50 µm diameter = 120 nm	anatase	[51]/2015
TiO ₂	Ti foil in NH ₄ F and (NH ₄) ₂ SO ₄ and deionized water Anodization = 20 V Time = 2 h Temp. = RT Thermal annealing at 750 °C for 4 h in air	Nanotubes	length = NA diameter = 50–80 nm	anatase	[68]/2020
p-Co ₃ O ₄ /n-TiO ₂	Ti foil, NH ₄ F ethylene glycol, cobalt (II) nitrate hexahydrate and water Anodization = 50 V Time = 1 h Temp. = 500 °C	Nanotubes	length = NA diameter = 80 nm	anatase	[48]/2018
Pd decorated TiO ₂	Ti foil in NH ₄ F and ethylene glycol. Anodization = 60 V Time = 45 min Temp. = RT Thermal annealing at 6 h at 500 °C in ambient air	Nanotubes	length = NA diameter = 40 nm	anatase	[69]/2016
PbS quantum dots/TiO ₂	Ti foil in ethylene glycol solution containing NH ₄ F and H ₂ O Pb(NO ₃) ₂ dissolved in methanol and Na ₂ S in methanol. Anodization = 50 V Time = 5 h Temp. = RT	Nanotubes	length = 18 µm diameter = 80 nm	anatase	[70]/2016
Ni and Pd-modified TiO ₂	Ti foil, NH ₄ F, ethylene glycol and water. NiCl ₂ and PdCl ₂ Anodization = 20 V Temp. = 300 C Time = 3 h	Nanotubes	diameter = 50–60 nm length = 470 nm	anatase	[71]/2015
TiO ₂	Ti foil and NH ₄ F with H ₂ O in ethylene glycol Anodization = 50 V Time = 3 h Temp. = RT	Nanotubes	diameter = 100 nm length = NA	anatase	[72]/2016
Co-doped TiO ₂	Ti foil in glycol solution with ammonium fluoride and deionized water. Anodization = 30 V Time 2 h Temp. = RT	Nanotubes	diameter = 110 nm length = NA	anatase	[73]/2019

Table 2. Cont.

Electrospinning					
TiO ₂	Titanium tetraisopropoxid (C ₁₂ H ₂₈ O ₄ Ti), ethanol, acetic acid Stirring time = 15 min Voltage = 18 kV Rate = 2 mL/min Calcination temp. = 300 °C, 500 °C, 700 °C, 900 °C TBT (tetrabutyl titanate), indium nitrate hydrate, ethanol, DMF	Nanofibers	lengths = NA diameters = 50 nm, 80 nm, 130 nm, 200 nm	anatase/rutile mixed phase	[40]/2015
In ₂ O ₃ beads @ TiO ₂ -In ₂ O ₃ composite	(dimethylformamide), PVP (polyvinylpyrrolidone) Stirring time = 6 h Voltage = 16.0 kV Rate = 0.25 mL·h ⁻¹	Nanofibers	lengths = tens of μm diameter = 150–250 nm	polycrystalline TiO ₂ -In ₂ O ₃ composite	[60]/(2015)
Nb ₂ O ₅ -TiO ₂	Titanium isopropoxide, polyvinylpyrrolidone, acetic acid, ethanol stirring time = 12 h Voltage = 18.0 kV, −4.0 kV Rate = 1.5 mL/h, Calcination temp. = 500 °C Tetrabutyl titanate, poly-vinylpyrrolidone, ethanol, acetic acid stirred time = 20 min Ti/V molar ratio of 4:1	Nanofibers	lengths = NA diameter = 121.3 nm	anatase/ rutile mixed phase	[58]/2019
TiO ₂ /V ₂ O ₅	Annealing Temp = 450 °C Dimethylformamide, ethanol stirring time = 10 min SnCl ₂ ·2H ₂ O stirring time = 8 h voltage = 18 kV	Nanofibers	length = μm range diameter = 60 nm	anatase/ rutile mixed phase	[74]/2016
TiO ₂ -SnO ₂		Nanofibers	N/A	rutile	[59]/2017

Table 3. Advantages and disadvantages of hydrothermal, electrochemical anodization and electrospinning techniques.

Hydrothermal		Electrochemical Anodization		Electrospinning	
Advantages	Disadvantages	Advantages	Disadvantages	Advantages	Disadvantages
Simple, easy and low-cost synthesis method	The reaction takes long time	Production of High quality of 1D nanostructures specially nanotubes	Mainly used for nanotubes growth	Ease to fabricated composites	Limited control of structure porosity
Production of High quality of 1D nanostructures specially nanorods	Utilization of highly concentrated NaOH solution	Ordered and aligned structure	The mass-produced is limited	High efficiency	Use of toxic solvents
The morphology is controlled by synthesis parameters	Difficult in achieving uniform size	high aspect ratio (length/diameter ratio)	Utilization of toxic electrolyte: Hydrofluoric acid HF	Process simplicity	-
Easy addition of additives for doping	length/diameter ratio is smaller than the ratio produced by electrochemical anodization	Growth at room temperature	high production cost	Mass production	-
-	-	Aspect ratio controlled by synthesis parameters	Difficulties in separation of film from substrate	-	-

4. Working Principles of TiO₂-Based Chemical Sensors

Most semiconductor-based gas sensors rely on the chemo-resistive effect—that is, the change of the electrical conductance or resistance upon the exposure to chemical compounds. In particular,

the semiconductor sensing element resistance can increase or decrease when reacting with oxidizing (O₃, CO₂ and NO₂) or reducing (H₂, H₂S, NH₃ and VOCs) gases [66,67,71,75,76]. The sensing mechanism of TiO₂-based chemical sensors is frequently explained by two processes: receptor and transduction function, as shown in Figure 8.

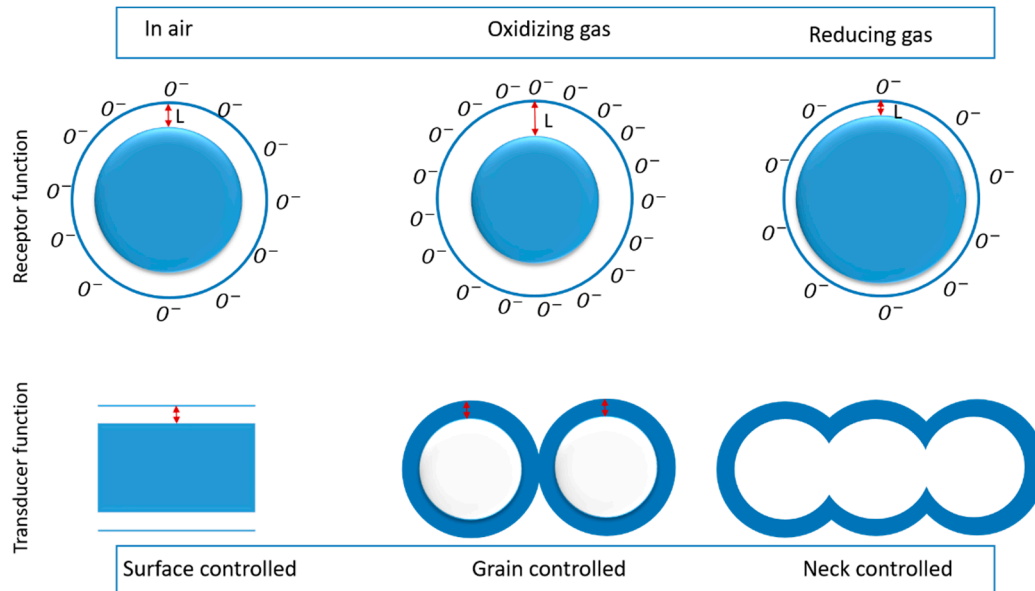
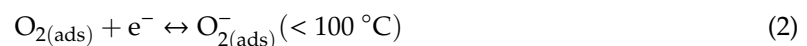


Figure 8. Schematic representation of gas sensing at different modes.

The receptor process takes place on the surface of TiO₂, comprising physisorption and chemisorption processes [77,78]. As TiO₂ surface is exposed to air, the oxygen molecules start to physically adsorb on its surface. This process is determined by dipole and van der Waals interactions. Furthermore, these adsorbed molecules initiate capturing electrons from the conduction band of TiO₂, while oxygen species chemisorb (O⁻, O₂⁻) on the surface. This chemisorption of oxygen ions creates a depletion region near the TiO₂ surface.

The receptor process efficiency is majorly dependent on physisorption and chemisorption processes, which in turn depend upon the sensor operating temperature. Specifically, at elevated temperature (100–500 °C), the chemisorption of oxygen ions occurs on the oxide surface and can be explained by the following equations [79]:



Hence, the type of chemisorbed oxygen ions depends on the sensors’ operating temperature and determines the reaction mechanism with the gas analyte. Due to this, metal oxides gas sensors are operated at different temperatures to find the optimal working conditions for each gas analyte.

Secondly, the transducer process is determined by the transportation of electrons in TiO₂ and their transformation into a readable electronic signal. This process is mainly divided into three different modes (shown in Figure 8), i.e., surface-controlled mode, grain-controlled mode and neck-controlled mode [77,78,80,81]. (i) The surface-controlled model is mainly related to compact thin film structures, in which the gases react to the surface of TiO₂ rather than the bulk. (ii) On the other hand, in the grain-neck-controlled model, the gases reactivity is much higher. This is due to the fact that in the

granular structures with higher porosity, each grain and neck boundary will create a depletion region that leads to an increase in the sensor resistance, thus improving the sensitivity of the TiO₂ nanostructures.

Furthermore, the surface to volume ratio, grain size and porosity of the fabricated TiO₂ nanostructures can majorly affect the above mention process. In this direction, in the last decade, different 1D nanostructures of TiO₂ and their heterostructures, as well as element doping of TiO₂, have been highly studied in chemical sensing applications [58,61,67,71,74].

5. Chemical Sensing Properties

5.1. Sensing of Reducing Gases

Among many metal oxides, 1D TiO₂ nanostructures have been extensively used as sensing materials to build a high-performance chemical sensor for the detection of reducing gases such as H₂, VOCs (ethanol, acetone etc.) H₂S, NH₃ and so on [40,71,72,78].

Among chemical compounds crucial to detect and monitor, H₂ is one of the most important. H₂ is used in applications such as fuel cells [82]; it is extremely flammable and explosive, and, therefore, its detection is crucial to guarantee a safe exploitation of H₂ based energy-related systems. M. Enachi et al. [67] reported the sensing performances of three different phases of TiO₂ nanotubes including amorphous, anatase and mixed anatase/rutile. The phase transition was achieved using thermal treatment by annealing the sample after the deposition procedure. The authors separated a single nanotube and transferred it to the chip containing Au metal contacts to study the suitability of an individual TiO₂ nanotube as a hydrogen sensor and to investigate the sensing performance for the three obtained phases. The sensing device based on single nanotubes with mixed anatase/rutile phase exhibited a faster response and recovery time of ~0.7 s and ~0.9 s, respectively, and the response (defined as $\frac{I_{H_2}}{I_{air}}$) was about 3.5 at room temperature.

In order to improve the sensing performances of 1D TiO₂, many strategies have been proposed in the literature, such as increasing the response and reducing the power consumption using photoactivation, improving the selectivity, enhancing the response and reducing the working temperature by functionalization TiO₂ with transition metals, and maximizing the sensitivity by bulk doping and by building heterojunctions.

A. Nikfarjam et al. proposed photoactivation as a method to increase the response of the thermoactivated TiO₂ nanofibers network [40]. The best response was found 18 and 96 towards 25 and 200 ppm of H₂, respectively, under UV illumination at 190 °C, significantly higher compared to 1.8 and 10.1 in dark at 290 °C. The sensor exhibited a fast response, and a long-term stability of 9 months was reported. Moreover, the optimal working temperature decreased from 290 to 190 °C. This increase in performance was attributed to the reduction of the activation energy between H₂ molecules and TiO₂ surface under UV irradiation, and to the increase in oxygen chemisorption (O⁻) density for its interaction with H₂, even at low temperatures. Such results are interesting for the possibility to achieve battery-operated devices thanks to the reduction in power consumption and miniaturization of the gas sensor device.

Another way to increase sensing performances is the functionalization of the TiO₂ surface. For example, TiO₂ nanorods produced using the hydrothermal method were modified with Pd nanoparticles [75]. Figure 9 shows Pd/TiO₂ NRs exhibiting a great enhancement toward 1000 ppm of H₂ at 200 °C with a 35-fold higher response compared with TiO₂ NTs due to the spillover effect. Specifically, Pd nanoparticles on the TiO₂ NRs catalytically stimulate the dissociation of molecular oxygen and atomic products obtained during this process diffuse to the metal oxide. This process greatly enhances the oxygen vacancies on the TiO₂ surface and directly affects the sensing performance. Furthermore, together with the good selectivity towards H₂ over other VOCs, the working temperature was reduced from 200 to 30 °C and the response increased to 250, thanks to the hydrogen collector activity of Pd.

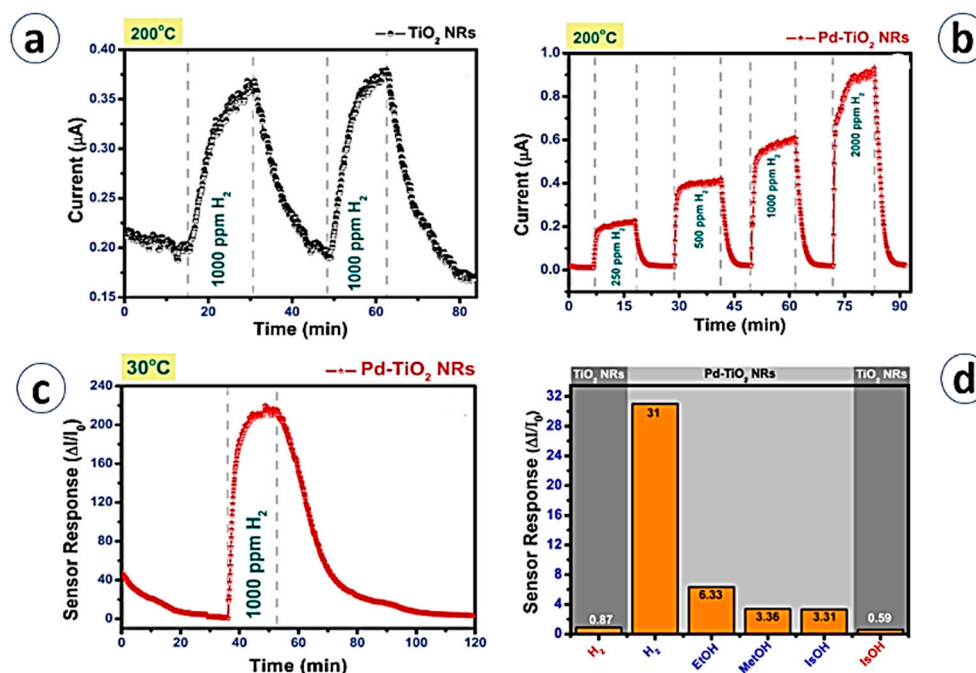


Figure 9. (a) Dynamic response of TiO₂ nanorods at 200 °C. (b) Dynamic response of Pd-TiO₂ at 200 °C toward different H₂ concentrations. (c) Dynamic response of Pd-TiO₂ at 30 °C toward 100 ppm of H₂ (d) Sensor responses of TiO₂ and Pd TiO₂ nanorod device for H₂ and VOCs at 200 °C. Reprinted with permission from Ref. [75] Copyright 2016 Elsevier.

Furthermore, the combination of two different catalysts may increase performance even more. Shoutian Ren et al. [45] achieved an enhancement in response and response time (350% and 42 s) for AuPd-TiO₂ as compared with Pd-TiO₂ (2% and 21 s) at room temperature. They also investigated the sensing mechanism by formation of a local heterostructure between Au and Pd, which enhanced electrocatalytic activity of alloyed macrostructures and increased the hydrogen dissociation process further; a crucial role was played by the size and the content of Pd/Au ratios. Moreover, heterostructures based on titanium oxide such as Co₃O₄/TiO₂ and CuO/TiO₂ also revealed high potentialities for hydrogen detection [48,49].

Other chemical species that deserve attention are volatile organic compounds (VOCs). VOCs, which commonly arise from painting, vehicle exhaust emissions and oil refining, are hazardous compounds. They have serious effects on air quality and human health. TiO₂ nanostructures have been investigated as VOC sensors. In particular, TiO₂ nanorods showed good sensing performances in triethylamine (TEA) detection [43]. The fast response time (2s), low detection limit (0.1 ppm) and good selectivity over acetone, ethanol, benzene, chlorobenzene, methanol and N-propanol make it a good choice for controlling fish and seafood freshness [43]. In this study, the sensing mechanism of TEA has been proved using XPS, confirming that TEA adsorbs on the surface of TiO₂ NRs before reacting with pre-adsorbed oxygen. Ethanol and acetone are the most studied among VOCs targets for 1D TiO₂ [83–85]. In this context, it has been shown that TiO₂ nanorods with a diameter of 500 nm show a good response of 9, 13 and 20 towards 10, 300 and 1000 ppm of acetone at 500 °C with response and recovery time ranging from 11 to 14 s and 4 to 8 s, respectively, showing a fast acetone detection [86]. TiO₂ nanotubes with 0.85 μm lengths and wall thickness of 13 nm show efficient low-temperature (150 °C) ethanol sensing with an 80% response exposed to 1000 ppm, and response and recovery times of 11 and 117 s, respectively [85].

However, in the last five years, greater interest was focused on heterostructured and composite titania material for the purpose of increasing their sensing performances. Siowwoon Ng et al. [47] investigated TiO₂/ZnO core-shell nanostructures for the development of ethanol sensors. In their work, a fascinating strategy has been employed to control the ZnO shell thickness (0.19, 1.9, 7.6 and

19 nm). The response of TiO₂/ZnO core shell nanostructures towards 1930 ppm of ethanol is improved by increasing the thickness of ZnO shell; with a 19 nm thickness, it is 11 times higher than the one of pristine TiO₂ NTs at 200 °C (Figure 10). The sensor response dynamics are enhanced, and good repeatability and stability have been achieved. Similar results have been established on 1D TiO₂ heterostructures with Nb₂O₅, Al₂O₃, V₂O₅ and TiO_{2-x} materials [58,61,74,87].

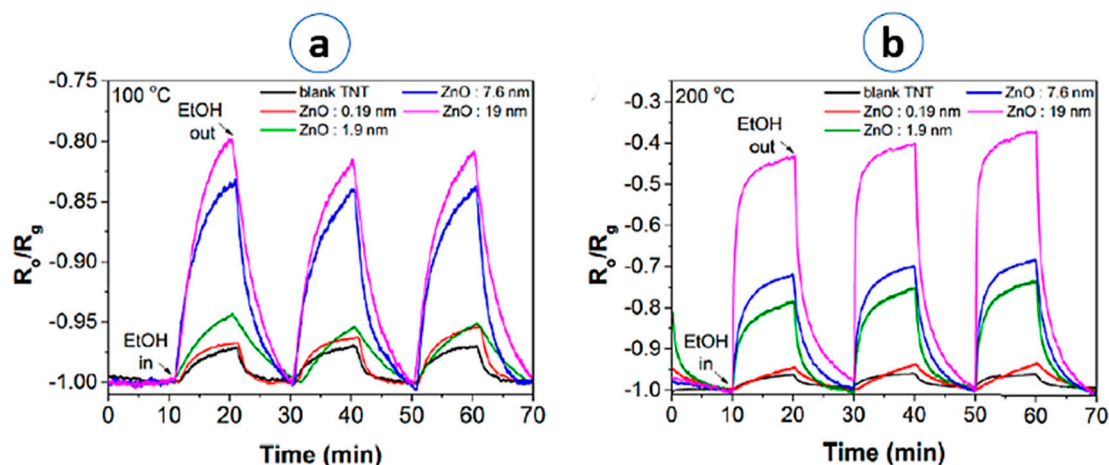


Figure 10. Ethanol sensing responses of TiO₂ NTs and TiO₂/ZnO (0.19, 1.9, 7.6 and 19 nm) core/shell (a) at 100 °C and (b) at 200 °C. Reprinted with permission from Ref. [47] Copyright 2018 WILEY.

Enhancing sensing performances of heterojunction are due to band bending at the interface attributed to Fermi level alignment via charge transfer; furthermore, active sites are provided for gas adsorption and synergistic reaction effects [47]. The improvement of sensing characteristics toward acetone have been investigated using different strategies, either by using heterojunction structure as reported by Feng Li et al., [59] who studied TiO₂/SnO₂ core shell nanofibers and observed a response improvement from 3 to 14 for TiO₂ and TiO₂/SnO₂, respectively, at 280 °C; by surface sensitization [71]; or sometimes by bulk doping [73].

1D TiO₂ also showed good potentialities as NH₃ and H₂S chemical sensors. Capability of detection of low concentrations of NH₃ at room temperature in different humidity environments has been proven [44]. The sensor exhibited good long-term stability (29 days), with a response of 102% toward 100 ppm of NH₃. Moreover, a decrease in response was observed by increasing humidity levels from 28% to 75%. The study also showed a good selectivity to NH₃ over CH₄, H₂S, NO₂, H₂, ethanol, methanol, acetone, diethylaniline (DEA) and TEA.

Another important chemical compound in terms of health, security and safety is H₂S. H₂S is a colorless gas that is very poisonous and extremely flammable. Exposure to H₂S concentration ranging from 20 to 100 ppm may cause eye burns and respiratory problems, and sometimes paralysis and even death [88,89]. Therefore, finding equipment for early detection of H₂S is highly recommended. In this context, P. M. Perillo et al. fabricated flexible H₂S sensors based on anatase TiO₂ nanotubes [72]. The tube length was 12 µm, while the pore and wall diameters were approximately 100 nm and 30 nm, respectively. The flexible sensor showed response of 75% towards 25 ppm of H₂S at room temperature with excellent long-term stability (6 months).

Table 4 reports a literature survey for the TiO₂ nanostructure and heterostructure growth procedures and their chemical/gas sensing performances towards reducing gases.

Table 4. Summary of the chemical/gas sensing properties of TiO₂-based nanostructures and heterostructures towards reducing gases.

Material	Synthesis Method	Target Gas/ Concentration	Response (S)	Temperature/ Humidity	Response/ Recovery Time	Ref./Year
TiO ₂ NTs	Electrochemical anodization	H ₂ /100 ppm	$S = (I_g/I_a)$ 3.5	RT/Dry air	0.7 s/0.9 s	[67]/2015
TiO ₂ NFs	Electrospinning	H ₂ /50 ppm	$S = (R_a/R_g)$ 30	190 °C with UV irradiation/Dry air	2s/6.9 s	[40]/2015
TiO ₂ NRs	Hydrothermal	H ₂ /2000 ppm	$S = (\Delta I/I \times 100)$ 215%	200 °C/Dry air	NA	[42]/2015
p-Co ₃ O ₄ /n-TiO ₂ NTs	Electrochemical anodization	H ₂ /1000 ppm	$S = (\Delta I/I)$ 6	200 °C/50%	10 min/5 min	[48]/2018
Pd decorated TiO ₂ NTs	Electrochemical anodization	H ₂ /10ppm	$S = (\Delta R/R)$ 1.25	180 °C/in dry synthetic air	20 s/40 s	[69]/2016
PdAu decorated TiO ₂ NWs	Hydrothermal	H ₂ /5 ppm	$S = (\Delta I/I \times 100)$ 350%	RT/-	42 s/NA	[45]/2016
TiO ₂ /ZnO core-shell NTs	Electrochemical anodization	Ethanol/1930 ppm	$S = (R_a/R_g)$ 0.8	100 °C/-	NA	[47]/2018
Al ₂ O ₃ /TiO ₂	Thermal oxidation	Ethanol/1000 ppm	$S = (R_a/R_g)$ 1108.9	650 °C/-	4 min/20 min	[61]/2017
Nb ₂ O ₅ -TiO ₂ NFs	Electrospinning	Ethanol/500 ppm	$S = (R_a/R_g)$ 21.64	250 °C/45%	NA	[58]/2019
TiO ₂ /V ₂ O ₅ NFs	Electrospinning	Ethanol/100 ppm	$S = (R_a/R_g)$ 24.6	350 °C/30%	6 s/7s	[74]/2016
Ni-TiO ₂ NTs	Electrochemical anodization	Acetone/1000 ppm	$S = (\Delta R/R \times 100)$ 82%	100 °C/-	NA	[71]/2015
TiO ₂ -SnO ₂ core-shell NFs	Electrospinning	Acetone/100 ppm	$S = (R_a/R_g)$ 13.5	280 °C/-	2 s/60 s	[59]/2017
TiO ₂ NTs	Electrochemical anodization	Acetone/50 vol%	$S = (\Delta R/R \times 100)$ 115%	Light irradiation at RT/-	NA	[68]/2020
TiO ₂ NWs	Vapor-Phase growth	CO/1 ppm	$S = (NA)$ 11%	400 °C/-	NA	[63]/2016
TiO ₂ NRs	Hydrothermal	Ammonia/20 ppm	$S = (\Delta R/R \times 100)$ 14.1%	RT/50%	61 s/9 s	[44]/ 2020
Pbs QDs/TiO ₂ NTs	Electrochemical anodization	Ammonia/100 ppm	$S = (R_a/R_g)$ 17.49	RT/-	NA	[70]/2016
TiO ₂ NTs	Electrochemical anodization	H ₂ S/6 to38 ppm	$S = (\Delta R/R \times 100)$ 12 to 144%	70 °C/10%	NA	[72]/2016
Co-doped TiO ₂ NTs	Electrochemical anodization	H ₂ S/50 ppm	$S = (R_a/R_g)$ 199.16%	300 °C/50%	15 s/4 s	[73]/2019

5.2. Sensing of Oxidizing Gases

Environmentally hazardous oxidizing compounds such as NO₂, O₃ and CO₂, etc. are among the major concerns for the human life and health [11,90–93]. For example, NO₂ is a typical air pollutant byproduct of combustion facilities, aircrafts and automobiles. According to the American standard air quality monitoring protocols for NO₂, the concentration should be detectable in the range of 3–25 ppm. Moreover, the decomposition of NO₂ by solar irradiation is a common source of ozone (O₃) production. The safe concentration of ozone is 50 ppb for continuous exposure and 100 ppb for short-term exposure has been set for the developed countries. Thus, a low-cost, reliable sensor with high selectivity and sensitivity is of huge demand for environmental safety and industrial control purposes. In this context, TiO₂ nanostructure-based sensors have been widely investigated for the detection of these hazardous pollutants [48,50,60,61,63–66,94].

A recent report by Z. Zhu et al. [66] presented highly sensitive NO₂ sensors based on TiO₂ nanowires. These hydrothermally grown nanowires-based TiO₂ sensors showed very fast response and recovery time of 10 to 19 s respectively, with a response of 3.1 towards 100 ppm of NO₂. Furthermore, TiO₂ nanorods-based sensors have been widely used for the investigation of highly sensitive NO₂ sensors. Z. Tshabalala et al. [64] presented a hydrothermal method followed by an annealing process to fabricated pristine TiO₂ NRs. Different devices were prepared using different washing solutions such as distilled water and hydrochloric acid of different concentrations 0.25, 0.5 and 1 M, and were annealed at different temperatures afterward. Gas tests, performed at RT in dry air, show that the sensing properties depend on washing solution and annealing temperature. The best response (1300

at 40 ppm of NO_2) was achieved by the samples cleaned with hydrochloric acid 1.0 M and annealed at 700 °C. The best optimized samples exhibit high porosity, which leads to the larger surface area, in turn increasing the response.

As discussed in pervious sections, in the last five years, much work has been done to achieve high sensing performance by doping of metal particles or by creating the oxide-to-oxide junction. D. Ponnuvelu et al. [94] reported on Au-decorated mixed phase TiO_2 NRs fabricated by hydrothermal method for highly sensitive NO_2 sensors. After Au particle decoration, not only did the response value increase, but also the working temperature decreased from 400 °C to 200 °C in comparison to bare TiO_2 NRs. The sensor devices were tested toward very low concentrations of NO_2 from 500 ppb to 5 ppm with a response of 135.5 to 15, respectively. The enhancement in NRs sensing performances is due to the catalytic effect of Au doping to the NRs surface that induces surface defects and the coexistence of mixed phases (metastable anatase and thermodynamically stable rutile) of TiO_2 .

Constructing a junction between two similar or dissimilar materials is another successful method to improve the sensing performance of metal oxide-based devices [60,65]. L. Wang et al. [60] presented an interesting report on TiO_2 - In_2O_3 composite nanofibers (NFs) with In_2O_3 porous beads built using the electrospinning method for the detection of NO_2 . In particular, they developed a single-step process, followed by calcination, to achieve a nanoparticle–nanofiber structure. The porous single crystal NRs loaded on the composite NFs play a crucial role in the formation of Schottky junctions between the semiconductor materials and the gold electrodes. These junctions reduce the interfacial resistance when charge carriers flow through the contacts, thus increasing the overall conductance (shown in Figure 11). Moreover, the surface defects along with the NFs porosity give birth to a high surface-to-volume ratio which allows the adsorption of gases (O_2 or NO_2) and the electrons capture more effectively, even in the bulk. The resulting sensing devices exhibit superior performances at RT with a response of 95 toward 97 ppm of NO_2 .

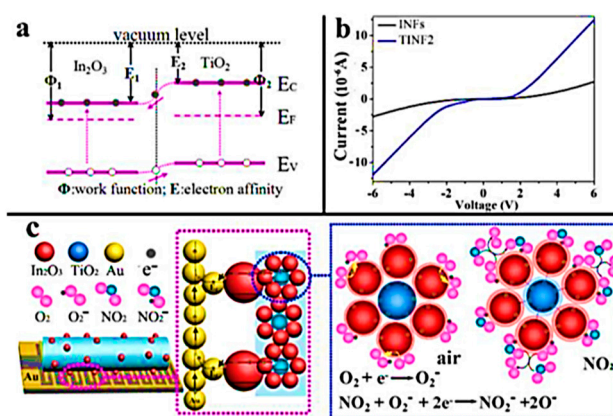


Figure 11. (a) Energy band diagram of In_2O_3 and TiO_2 , EC: conduction band and EV: valence band; (b) I-V curves measured for INFs and TINiF_2 thin film sensors in air at RT, which were treated at 110 °C (the gate voltage $V_g = 0.1$); (c) The gas sensing reactions based on Schottky junction between Au electrode and In_2O_3 beads. Reprinted with permission from Ref. [46] Copyright 2015 American Chemical Society.

Even though oxygen is not a toxic gas, the results reported by Wang et al. [95] from fabricating TiO_2 NRs array using an acid vapor oxidation (AVO) technique are worth mentioning. The sensing tests were carried out in dry air at RT for O_2 concentrations ranging from 1% to 16% (volume ratio). The responses were monotonically increasing with the concentration approaching 2.1 at 16%. At the same concentration, the best tradeoff between response and recovery time (55 s and 51 s) were obtained. These sensors have also demonstrated a good repeatability and selectivity against hydrogen and methane.

Table 5 comprises the literature survey for TiO_2 nanostructures and heterostructures together with their growth techniques and sensing performance towards oxidizing gases.

Table 5. Summary of the gas sensing properties of TiO₂-based nanostructure and heterostructure sensors towards oxidizing gases.

Material	Synthesis Method	Target Gas/ Concentration	Response (S)	Temperature/ Humidity	Response/ Recovery Time	Ref./Year
TiO ₂ NWs	Hydrothermal	NO ₂ /100 ppm	$S = (R_a/R_g)$ 3.1	RT/50%RH	10 s/19 s	[66]/(2018)
TiO ₂ NRs	Hydrothermal and annealing	NO ₂ /40 ppm	$S = (R_g/R_a)$ 1300	RT/dry air	NA	[64]/(2017)
TiO ₂ -Al ₂ O ₃ Core-shell NWs	Thermal oxidation	NO ₂ /1000 ppm	$S = (R_g/R_a)$ 1.9	650 °C/dry air	180 s/180 s	[61]/(2017)
MoS ₂ -Decorated TiO ₂ NTs	Anodization and Hydrothermal	NO ₂ /100 ppm	$S = (R_g/R_a)$ 1.1	150 °C/45%RH	NA	[50]/(2016)
TiO ₂ -In ₂ O ₃ Composite NFs	Electrospinning	NO ₂ /97 ppm	$S = (\Delta R/R_a)$ 95	RT/26%RH	6.7 s/NA	[60]/(2015)
TiO ₂ NTs	Anodization	NO ₂ /50 ppm	$S = (\Delta I/I_g)$ 17	200 °C/50%RH	NA	[48]/(2018)
TiO ₂ Networked NWs	Vapor-phase growth	NO ₂ /50 ppm	$S = (\Delta R/R_a \times 100)$ 8%	400 °C/dry air	NA	[63]/(2016)
TiO ₂ -Ag ₂ O Composite NRs	Hydrothermal and sputtering	NO ₂ /0.5 ppm	$S = (R_g/R_a)$ 3.1	250 °C/dry air	87 s/112 s	[65]/(2019)
TiO ₂ @Au Heterojunction NRs	Hydrothermal and chemical approach	NO ₂ /5 ppm	$S = (\Delta R/R_a)$ 135.5	250 °C/dry air	40 s/43 s	[94]/(2017)
TiO ₂ NRs Array	Acid vapor oxidation	O ₂ /16% vol.	$S = (R_g/R_a)$ 2.1	RT/dry air	55 s/51 s	[95]/(2016)

5.3. Effect of Humidity

Generally, the response of the metal oxides gas sensor in the presence of humidity is reduced. The reduction in their gas sensing response in a wet environment occurs due to the competition of adsorption between the analyte and the water molecules. The moisture may adsorb on the surface metal sites, reducing oxygen adsorption. In addition, hydrogen produced by the homolytic dissociation of water molecules subsequently reacts with the lattice oxygen of the metal oxides (MOX), forming surface hydroxyl species. Hence, in the presence of humidity, water is in competition with the absorption of hydrogen at the MOX surface. The reduction in the gas sensing response in a wet environment is commonly known as the “poisoning effect of water on metal oxide sensors” [96,97]. Moreover, at elevated temperatures, moisture may also be responsible for a restructuring of the surfaces, modifying the density of oxygen absorption sites.

6. Conclusions

Titanium oxide (TiO₂) is a nontoxic and environmentally friendly material in nature with excellent biocompatibility and stability, which allows its nanomaterials to be adopted in a wide range of applications, especially in chemical/gas sensing. The 1D TiO₂ nanostructures such as nanowires, nanotubes and nanofibers possess larger specific surface areas that contribute to the unique physical, chemical, optical and electronic properties of this material. TiO₂-based 1D nanostructures have been grown using large-scale and high-yield techniques such as hydrothermal, electrochemical anodization and the electrospinning growth method showed exceptional sensing performances for the detection of different gas analytes such as VOCs, toxic and explosive gases. However, in the last five to seven years, great attention has been paid to improving the sensing performance of these nanostructures by doping of metal nanoparticle or by creating a junction of different MOX. These heterostructures show an enhancement in sensitivity, selectivity and lower operating temperature with faster responses and recovery times. The change in sensing performances of composite structures compared to pristine TiO₂ is attributed to the heterojunction formation within the interface of two semiconducting materials, as well as catalytical and synergetic effects. Furthermore, the formation of nanostructured material also influences gas adsorption and diffusion, which leads to a change in sensing performances.

Concluding, in the field of chemical/gas sensing, there has been much progress achieved in growth of various 1D TiO₂ nanostructures and heterostructures using different fabrication techniques.

The effect of different phases of TiO₂ on its sensing properties has been widely investigated. In this review, we have presented the recent achievements in the field of TiO₂-based 1D nanostructures fabrication and understanding of their sensing mechanism and their sensing performance related to different gas analytes.

Author Contributions: Conceptualization, N.K., M.S., A.M., E.C. and G.D.; writing of the original draft preparation, N.K. and E.C. writing of review and editing, E.C.; validation, E.C.; visualization, E.C.; supervision, E.C.; project administration, E.C.; funding acquisition, N.K., M.S., A.M., E.C. and G.D. All authors have read and agreed to the published version of the manuscript.

Funding: This work was partially funded by MIUR “Smart Cities and Communities and social innovation” project titled “SWaRM Net/Smart Water Resource Management—Networks and by the NATO Science for Peace and Security Programmer (SPS) under grant G5634 AMOXES—“Advanced Electro-Optical Chemical Sensors”.

Conflicts of Interest: The authors declare no conflict of interest. The funders had no role in the design of the study; in the collection, analyses, or interpretation of data; in the writing of the manuscript, or in the decision to publish the results.

References

1. Comini, E. Metal oxide nanowire chemical sensors: Innovation and quality of life. *Mater. Today* **2016**, *19*, 559–567. [[CrossRef](#)]
2. Zhou, Z.; Lan, C.; Wei, R.; Ho, J.C. Transparent metal-oxide nanowires and their applications in harsh electronics. *J. Mater. Chem. C* **2019**, *7*, 202–217. [[CrossRef](#)]
3. Comini, E.; Bianchi, S.; Faglia, G.; Ferroni, M.; Vomiero, A.; Sberveglieri, G. Functional nanowires of tin oxide. *Appl. Phys. A* **2007**, *89*, 73–76. [[CrossRef](#)]
4. Shen, Y.; Yamazaki, T.; Liu, Z.; Meng, D.; Kikuta, T.; Nakatani, N.; Saito, M.; Mori, M. Microstructure and H₂ gas sensing properties of undoped and Pd-doped SnO₂ nanowires. *Sens. Actuators B Chem.* **2009**, *135*, 524–529. [[CrossRef](#)]
5. Suman, P.H.; Felix, A.A.; Tuller, H.L.; Varela, J.A.; Orlandi, M.O. Comparative gas sensor response of SnO₂, SnO and Sn₃O₄ nanobelts to NO₂ and potential interferences. *Sens. Actuators B Chem.* **2015**, *208*, 122–127. [[CrossRef](#)]
6. Sharma, A.P.; Dhakal, P.; Pradhan, D.K.; Behera, M.K.; Xiao, B.; Baha, M. Fabrication and characterization of SnO₂ nanorods for room temperature gas sensors. *AIP Adv.* **2018**, *8*, 095219. [[CrossRef](#)]
7. Forleo, A.; Francioso, L.; Capone, S.; Casino, F.; Siciliano, P.; Tan, O.K.; Hui, H. Wafer-Level Fabrication and Gas Sensing Properties of miniaturized gas sensors based on Inductively Coupled Plasma Deposited Tin Oxide Nanorods. *Procedia Chem.* **2009**, *1*, 196–199. [[CrossRef](#)]
8. Qian, L.H.; Wang, K.; Li, Y.; Fang, H.T.; Lu, Q.H.; Ma, X.L. CO sensor based on Au-decorated SnO₂ nanobelt. *Mater. Chem. Phys.* **2006**, *100*, 82–84. [[CrossRef](#)]
9. Kaur, N.; Singh, M.; Comini, E. One-Dimensional Nanostructured Oxide Chemosensitive Sensors. *Langmuir* **2020**, *36*, 6326–6344. [[CrossRef](#)]
10. Kaur, N.; Comini, E.; Zappa, D.; Poli, N.; Sberveglieri, G. Nickel oxide nanowires: Vapor liquid solid synthesis and integration into a gas sensing device. *Nanotechnology* **2016**, *27*, 205701. [[CrossRef](#)]
11. Kaur, N.; Zappa, D.; Poli, N.; Comini, E. Integration of VLS-Grown WO₃ Nanowires into Sensing Devices for the Detection of H₂S and O₃. *ACS Omega* **2019**, *4*, 16336–16343. [[CrossRef](#)] [[PubMed](#)]
12. Asiah, M.N.; Mamat, M.H.; Khusaimi, Z.; Achoi, M.F.; Abdullah, S.; Rusop, M. Thermal stability and phase transformation of TiO₂ nanowires at various temperatures. *Microelectron. Eng.* **2013**, *108*, 134–137. [[CrossRef](#)]
13. Fàbrega, C.; Casals, O.; Hernández-Ramírez, F.; Prades, J.D. A review on efficient self-heating in nanowire sensors: Prospects for very-low power devices. *Sens. Actuators B Chem.* **2018**, *256*, 797–811. [[CrossRef](#)]
14. Baratto, C.; Comini, E.; Ferroni, M.; Faglia, G.; Sberveglieri, G. Plasma-induced enhancement of UV photoluminescence in ZnO nanowires. *CrystEngComm* **2013**, *15*, 7981. [[CrossRef](#)]
15. Kaur, N.; Comini, E.; Poli, N.; Zappa, D.; Sberveglieri, G. Nickel Oxide Nanowires Growth by VLS Technique for Gas Sensing Application. *Procedia Eng.* **2015**, *120*, 760–763. [[CrossRef](#)]
16. Topcu, S.; Jodhani, G.; Gouma, P. Optimized Nanostructured TiO₂ Photocatalysts. *Front. Mater.* **2016**, *3*, 35. [[CrossRef](#)]

17. Mavrič, T.; Benčina, M.; Imani, R.; Junkar, I.; Valant, M.; Kralj-Iglič, V.; Iglič, A. Electrochemical Biosensor Based on TiO₂ Nanomaterials for Cancer Diagnostics. In *Advances in Biomembranes and Lipid Self-Assembly*; Elsevier B.V.: Cambridge, MA, USA, 2018; Volume 27, pp. 63–105.
18. Maziarz, W.; Kusior, A.; Trenczek-Zajac, A. Nanostructured TiO₂-based gas sensors with enhanced sensitivity to reducing gases. *Beilstein J. Nanotechnol.* **2016**, *7*, 1718–1726. [[CrossRef](#)]
19. Bai, Y.; Mora-Seró, I.; De Angelis, F.; Bisquert, J.; Wang, P. Titanium Dioxide Nanomaterials for Photovoltaic Applications. *Chem. Rev.* **2014**, *114*, 10095–10130. [[CrossRef](#)]
20. Wang, Y.; Zu, M.; Zhou, X.; Lin, H.; Peng, F.; Zhang, S. Designing efficient TiO₂-based photoelectrocatalysis systems for chemical engineering and sensing. *Chem. Eng. J.* **2020**, *381*, 122605. [[CrossRef](#)]
21. Mardare, D.; Cornei, N.; Mita, C.; Florea, D.; Stancu, A.; Tiron, V.; Manole, A.; Adomnitei, C. Low temperature TiO₂ based gas sensors for CO₂. *Ceram. Int.* **2016**, *42*, 7353–7359. [[CrossRef](#)]
22. Cui, H.-F.; Wu, W.-W.; Li, M.-M.; Song, X.; Lv, Y.; Zhang, T.-T. A highly stable acetylcholinesterase biosensor based on chitosan-TiO₂-graphene nanocomposites for detection of organophosphate pesticides. *Biosens. Bioelectron.* **2018**, *99*, 223–229. [[CrossRef](#)] [[PubMed](#)]
23. Kim, Y.C.; Lee, K.H.; Sasaki, S.; Hashimoto, K.; Ikebukuro, K.; Karube, I. Photocatalytic sensor for chemical oxygen demand determination based on oxygen electrode. *Anal. Chem.* **2000**, *72*, 3379–3382. [[CrossRef](#)] [[PubMed](#)]
24. Li, X.; Yin, W.; Li, J.; Bai, J.; Huang, K.; Li, J.; Zhou, B. TiO₂ Nanotube Sensor for Online Chemical Oxygen Demand Determination in Conjunction with Flow Injection Technique. *Water Environ. Res.* **2014**, *86*, 532–539. [[CrossRef](#)] [[PubMed](#)]
25. Bai, J.; Zhou, B. Titanium Dioxide Nanomaterials for Sensor Applications. *Chem. Rev.* **2014**, *114*, 10131–10176. [[CrossRef](#)] [[PubMed](#)]
26. Diebold, U. The surface science of titanium dioxide. *Surf. Sci. Rep.* **2003**, *48*, 53–229. [[CrossRef](#)]
27. Kumar, S.G.; Rao, K.S.R.K. Polymorphic phase transition among the titania crystal structures using a solution-based approach: From precursor chemistry to nucleation process. *Nanoscale* **2014**, *6*, 11574–11632. [[CrossRef](#)]
28. Xu, J.; Wu, S.; Jin, J.; Peng, T. Preparation of brookite TiO₂ nanoparticles with small sizes and the improved photovoltaic performance of brookite-based dye-sensitized solar cells. *Nanoscale* **2016**, *8*, 18771–18781. [[CrossRef](#)]
29. Zhang, W.; Shen, D.; Liu, Z.; Wu, N.-L.; Wei, M. Brookite TiO₂ mesocrystals with enhanced lithium-ion intercalation properties. *Chem. Commun.* **2018**, *54*, 11491–11494. [[CrossRef](#)]
30. Gupta, S.M.; Tripathi, M. A review of TiO₂ nanoparticles. *Chinese Sci. Bull.* **2011**, *56*, 1639. [[CrossRef](#)]
31. El Goresy, A.; Chen, M.; Gillet, P.; Dubrovinsky, L.; Graup, G.; Ahuja, R. A natural shock-induced dense polymorph of rutile with α -PbO₂ structure in the suevite from the Ries crater in Germany. *Earth Planet. Sci. Lett.* **2001**, *192*, 485–495. [[CrossRef](#)]
32. Karthick, S.N.; Hemalatha, K.V.; Balasingam, S.K.; Manik Clinton, F.; Akshaya, S.; Kim, H. Dye-Sensitized Solar Cells: History, Components, Configuration, and Working Principle. In *Interfacial Engineering in Functional Materials for Dye-Sensitized Solar Cells*; Wiley: Hoboken, NJ, USA, 2019; pp. 1–16.
33. Van de Krol, R. Erratum: “Mott-Schottky Analysis of Nanometer-Scale Thin-Film Anatase TiO₂” [*J. Electrochem. Soc.*, **144**, 1723 (1997)]. *J. Electrochem. Soc.* **1998**, *145*, 3697. [[CrossRef](#)]
34. Carp, O.; Huisman, C.L.; Reller, A. Photoinduced reactivity of titanium dioxide. *Prog. Solid State Chem.* **2004**, *32*, 33–177. [[CrossRef](#)]
35. Shi, J.; Wang, X. Growth of rutile titanium dioxide nanowires by pulsed chemical vapor deposition. *Cryst. Growth Des.* **2011**, *11*, 949–954. [[CrossRef](#)]
36. Kemell, M.; Pore, V.; Tupala, J.; Ritala, M.; Leskelä, M. Atomic layer deposition of nanostructured TiO₂ photocatalysts via template approach. *Chem. Mater.* **2007**, *19*, 1816–1820. [[CrossRef](#)]
37. Maijenburg, A.W.; Veerbeek, J.; De Putter, R.; Veldhuis, S.A.; Zoontjes, M.G.C.; Mul, G.; Montero-Moreno, J.M.; Nielsch, K.; Schäfer, H.; Steinhart, M.; et al. Electrochemical synthesis of coaxial TiO₂-Ag nanowires and their application in photocatalytic water splitting. *J. Mater. Chem. A* **2014**, *2*, 2648–2656. [[CrossRef](#)]
38. Zhao, B.; Lin, L.; He, D. Phase and morphological transitions of titania/titanate nanostructures from an acid to an alkali hydrothermal environment. *J. Mater. Chem. A* **2013**, *1*, 1659–1668. [[CrossRef](#)]
39. Rodríguez-Reyes, M.; Dorantes-Rosales, H.J. A simple route to obtain TiO₂ nanowires by the sol-gel method. *J. Sol Gel Sci. Technol.* **2011**, *59*, 658–661. [[CrossRef](#)]

40. Nikfarjam, A.; Salehifar, N. Improvement in gas-sensing properties of TiO₂ nanofiber sensor by UV irradiation. *Sens. Actuators B Chem.* **2015**, *211*, 146–156. [[CrossRef](#)]
41. Cushing, B.L.; Kolesnichenko, V.L.; O'Connor, C.J. Recent advances in the liquid-phase syntheses of inorganic nanoparticles. *Chem. Rev.* **2004**, *104*, 3893–3946. [[CrossRef](#)]
42. Alev, O.; Şennik, E.; Kiliç, N.; Öztürk, Z.Z. Gas sensor application of hydrothermally growth TiO₂ nanorods. *Procedia Eng.* **2015**, *120*, 1162–1165. [[CrossRef](#)]
43. Yang, H.Y.; Cheng, X.L.; Zhang, X.F.; Zheng, Z.K.; Tang, X.F.; Xu, Y.M.; Gao, S.; Zhao, H.; Huo, L.H. A novel sensor for fast detection of triethylamine based on rutile TiO₂ nanorod arrays. *Sens. Actuators B Chem.* **2014**, *205*, 322–328. [[CrossRef](#)]
44. Zhao, G.; Xuan, J.; Gong, Q.; Wang, L.; Ren, J.; Sun, M.; Jia, F.; Yin, G.; Liu, B. In Situ Growing Double-Layer TiO₂ Nanorod Arrays on New-Type FTO Electrodes for Low-Concentration NH₃ Detection at Room Temperature. *ACS Appl. Mater. Interfaces* **2020**, *12*, 8573–8582. [[CrossRef](#)] [[PubMed](#)]
45. Ren, S.; Liu, W. One-step photochemical deposition of PdAu alloyed nanoparticles on TiO₂ nanowires for ultra-sensitive H₂ detection. *J. Mater. Chem. A* **2016**, *4*, 2236–2245. [[CrossRef](#)]
46. Alam, U.; Fleisch, M.; Kretschmer, I.; Bahnemann, D.; Muneer, M. One-step hydrothermal synthesis of Bi-TiO₂ nanotube/graphene composites: An efficient photocatalyst for spectacular degradation of organic pollutants under visible light irradiation. *Appl. Catal. B Environ.* **2017**, *218*, 758–769. [[CrossRef](#)]
47. Ng, S.; Kuberský, P.; Krbal, M.; Prikryl, J.; Gärtnerová, V.; Moravcová, D.; Sopha, H.; Zazpe, R.; Yam, F.K.; Jäger, A.; et al. ZnO Coated Anodic 1D TiO₂ Nanotube Layers: Efficient Photo-Electrochemical and Gas Sensing Heterojunction. *Adv. Eng. Mater.* **2018**, *20*, 1700589. [[CrossRef](#)]
48. Alev, O.; Kılıç, A.; Çakırlar, Ç.; Büyükköse, S.; Öztürk, Z. Gas Sensing Properties of p-Co₃O₄/n-TiO₂ Nanotube Heterostructures. *Sensors* **2018**, *18*, 956. [[CrossRef](#)]
49. Alev, O.; Şennik, E.; Öztürk, Z.Z. Improved gas sensing performance of p-copper oxide thin film/n-TiO₂ nanotubes heterostructure. *J. Alloys Compd.* **2018**, *749*, 221–228. [[CrossRef](#)]
50. Zhao, P.X.; Tang, Y.; Mao, J.; Chen, Y.X.; Song, H.; Wang, J.W.; Song, Y.; Liang, Y.Q.; Zhang, X.M. One-Dimensional MoS₂-Decorated TiO₂ nanotube gas sensors for efficient alcohol sensing. *J. Alloys Compd.* **2016**, *674*, 252–258. [[CrossRef](#)]
51. Sopha, H.; Hromadko, L.; Nechvilova, K.; Macak, J.M. Effect of electrolyte age and potential changes on the morphology of TiO₂ nanotubes. *J. Electroanal. Chem.* **2015**, *759*, 122–128. [[CrossRef](#)]
52. Varghese, O.K.; Paulose, M.; Grimes, C.A. Long vertically aligned titania nanotubes on transparent conducting oxide for highly efficient solar cells. *Nat. Nanotechnol.* **2009**, *4*, 592–597. [[CrossRef](#)]
53. Munirathinam, B.; Pydimukkala, H.; Ramaswamy, N.; Neelakantan, L. Influence of crystallite size and surface morphology on electrochemical properties of annealed TiO₂ nanotubes. *Appl. Surf. Sci.* **2015**, *355*, 1245–1253. [[CrossRef](#)]
54. Mazierski, P.; Nischk, M.; Gołkowska, M.; Lisowski, W.; Gazda, M.; Winiarski, M.J.; Klimczuk, T.; Zaleska-Medynska, A. Photocatalytic activity of nitrogen doped TiO₂ nanotubes prepared by anodic oxidation: The effect of applied voltage, anodization time and amount of nitrogen dopant. *Appl. Catal. B Environ.* **2016**, *196*, 77–88. [[CrossRef](#)]
55. Bhardwaj, N.; Kundu, S.C. Electrospinning: A fascinating fiber fabrication technique. *Biotechnol. Adv.* **2010**, *28*, 325–347. [[CrossRef](#)]
56. Zhou, M.; Liu, Y.; Wu, B.; Zhang, X. Different crystalline phases of aligned TiO₂ nanowires and their ethanol gas sensing properties. *Phys. E Low Dimens. Syst. Nanostruct.* **2019**, *114*, 113601. [[CrossRef](#)]
57. Wang, S.; Lin, Z.X.; Wang, W.H.; Kuo, C.L.; Hwang, K.C.; Hong, C.C. Self-regenerating photocatalytic sensor based on dielectrophoretically assembled TiO₂ nanowires for chemical vapor sensing. *Sens. Actuators B Chem.* **2014**, *194*, 1–9. [[CrossRef](#)]
58. Li, G.; Zhang, X.; Lu, H.; Yan, C.; Chen, K.; Lu, H.; Gao, J.; Yang, Z.; Zhu, G.; Wang, C.; et al. Ethanol sensing properties and reduced sensor resistance using porous Nb₂O₅-TiO₂ n-n junction nanofibers. *Sens. Actuators B Chem.* **2019**, *283*, 602–612. [[CrossRef](#)]
59. Li, F.; Gao, X.; Wang, R.; Zhang, T.; Lu, G. Study on TiO₂-SnO₂ core-shell heterostructure nanofibers with different work function and its application in gas sensor. *Sens. Actuators B Chem.* **2017**, *248*, 812–819. [[CrossRef](#)]

60. Wang, L.; Gao, J.; Wu, B.; Kan, K.; Xu, S.; Xie, Y.; Li, L.; Shi, K. Designed Synthesis of In₂O₃ Beads@TiO₂-In₂O₃ Composite Nanofibers for High Performance NO₂ Sensor at Room Temperature. *ACS Appl. Mater. Interfaces* **2015**, *7*, 27152–27159. [[CrossRef](#)]
61. Arafat, M.M.; Haseeb, A.S.M.A.; Akbar, S.A.; Quadir, M.Z. In-situ fabricated gas sensors based on one dimensional core-shell TiO₂-Al₂O₃ nanostructures. *Sens. Actuators B Chem.* **2017**, *238*, 972–984. [[CrossRef](#)]
62. Wang, H.; Yao, Y.; Wu, G.; Sun, Q.; Wang, M.; Chen, X.; Wang, J. A room temperature oxygen gas sensor based on hierarchical TiO₂. In Proceedings of the IEEE 3M-NANO 2016–6th IEEE International Conference on Manipulation, Manufacturing and Measurement on the Nanoscale, Chongqing, China, 18–22 July 2016; Institute of Electrical and Electronics Engineers Inc.: Piscataway, NJ, USA; pp. 199–202.
63. Lee, J.S.; Katoch, A.; Kim, J.H.; Kim, S.S. Growth of networked TiO₂ nanowires for gas-sensing applications. *J. Nanosci. Nanotechnol.* **2016**, *16*, 11580–11585. [[CrossRef](#)]
64. Tshabalala, Z.P.; Shingange, K.; Dhonge, B.P.; Ntwaeaborwa, O.M.; Mhlongo, G.H.; Motaung, D.E. Fabrication of ultra-high sensitive and selective CH₄ room temperature gas sensing of TiO₂ nanorods: Detailed study on the annealing temperature. *Sens. Actuators B Chem.* **2017**, *238*, 402–419. [[CrossRef](#)]
65. Liang, Y.C.; Liu, Y.C. Design of nanoscaled surface morphology of TiO₂-Ag₂O composite nanorods through sputtering decoration process and their low-concentration NO₂ gas-sensing behaviors. *Nanomaterials* **2019**, *9*, 1150. [[CrossRef](#)] [[PubMed](#)]
66. Zhu, Z.; Lin, S.J.; Wu, C.H.; Wu, R.J. Synthesis of TiO₂ nanowires for rapid NO₂ detection. *Sens. Actuators A Phys.* **2018**, *272*, 288–294. [[CrossRef](#)]
67. Enachi, M.; Lupan, O.; Braniste, T.; Sarua, A.; Chow, L.; Mishra, Y.K.; Gedamu, D.; Adelong, R.; Tiginyanu, I. Integration of individual TiO₂ nanotube on the chip: Nanodevice for hydrogen sensing. *Phys. Status Solidi—Rapid Res. Lett.* **2015**, *9*, 171–174. [[CrossRef](#)]
68. Kumar, K.G.; Avinash, B.S.; Rahimi-Gorji, M.; Majdoubi, J. Photocatalytic activity and smartness of TiO₂ nanotube arrays for room temperature acetone sensing. *J. Mol. Liq.* **2020**, *300*, 112418. [[CrossRef](#)]
69. Moon, J.; Hedman, H.P.; Kemell, M.; Tuominen, A.; Punkkinen, R. Hydrogen sensor of Pd-decorated tubular TiO₂ layer prepared by anodization with patterned electrodes on SiO₂/Si substrate. *Sens. Actuators B Chem.* **2016**, *222*, 190–197. [[CrossRef](#)]
70. Liu, Y.; Wang, L.; Wang, H.; Xiong, M.; Yang, T.; Zakharova, G.S. Highly sensitive and selective ammonia gas sensors based on PbS quantum dots/TiO₂ nanotube arrays at room temperature. *Sens. Actuators B Chem.* **2016**, *236*, 529–536. [[CrossRef](#)]
71. Bhattacharyya, P.; Bhowmik, B.; Fecht, H.J. Operating Temperature, Repeatability, and Selectivity of TiO₂ Nanotube-Based Acetone Sensor: Influence of Pd and Ni Nanoparticle Modifications. *IEEE Trans. Device Mater. Reliab.* **2015**, *15*, 376–383. [[CrossRef](#)]
72. Perillo, P.M.; Rodríguez, D.F. TiO₂ nanotubes membrane flexible sensor for low-temperature H₂S detection. *Chemosensors* **2016**, *4*, 15. [[CrossRef](#)]
73. Tong, X.; Shen, W.; Chen, X. Enhanced H₂S sensing performance of cobalt doped free-standing TiO₂ nanotube array film and theoretical simulation based on density functional theory. *Appl. Surf. Sci.* **2019**, *469*, 414–422. [[CrossRef](#)]
74. Wang, Y.; Zhou, Y.; Meng, C.; Gao, Z.; Cao, X.; Li, X.; Xu, L.; Zhu, W.; Peng, X.; Zhang, B.; et al. A high-response ethanol gas sensor based on one-dimensional TiO₂/V₂O₅ branched nanoheterostructures. *Nanotechnology* **2016**, *27*, 425503. [[CrossRef](#)] [[PubMed](#)]
75. Şennik, E.; Alev, O.; Öztürk, Z.Z. The effect of Pd on the H₂ and VOC sensing properties of TiO₂ nanorods. *Sens. Actuators B Chem.* **2016**, *229*, 692–700. [[CrossRef](#)]
76. Kusior, A.; Radecka, M.; Zych, L.; Zakrzewska, K.; Reszka, A.; Kowalski, B.J. Sensitization of TiO₂/SnO₂ nanocomposites for gas detection. *Sens. Actuators B Chem.* **2013**, *189*, 251–259. [[CrossRef](#)]
77. Zakrzewska, K. Gas sensing mechanism of TiO₂-based thin films. *Pergamon* **2004**, *74*, 335–338. [[CrossRef](#)]
78. Galstyan, V.; Comini, E.; Faglia, G.; Sberveglieri, G. TiO₂ Nanotubes: Recent Advances in Synthesis and Gas Sensing Properties. *Sensors* **2013**, *13*, 14813–14838. [[CrossRef](#)]
79. Li, Z.; Li, H.; Wu, Z.; Wang, M.; Luo, J.; Torun, H.; Hu, P.; Yang, C.; Grundmann, M.; Liu, X.; et al. Advances in designs and mechanisms of semiconducting metal oxide nanostructures for high-precision gas sensors operated at room temperature. *Mater. Horizons* **2019**, *6*, 470–506. [[CrossRef](#)]
80. Göpel, W.; Schierbaum, K.D. SnO₂ sensors: Current status and future prospects. *Sens. Actuators B Chem.* **1995**, *26*, 1–12. [[CrossRef](#)]

81. Williams, D.E. Semiconducting oxides as gas-sensitive resistors. *Sens. Actuators B Chem.* **1999**, *57*, 1–16. [[CrossRef](#)]
82. Staffell, I.; Scamman, D.; Velazquez Abad, A.; Balcombe, P.; Dodds, P.E.; Ekins, P.; Shah, N.; Ward, K.R. The role of hydrogen and fuel cells in the global energy system. *Energy Environ. Sci.* **2019**, *12*, 463–491. [[CrossRef](#)]
83. Sabri, Y.M.; Kandjani, A.E.; Rashid, S.S.A.A.H.; Harrison, C.J.; Ippolito, S.J.; Bhargava, S.K. Soot template TiO₂ fractals as a photoactive gas sensor for acetone detection. *Sens. Actuators B Chem.* **2018**, *275*, 215–222. [[CrossRef](#)]
84. Avinash, B.S.; Chaturmukha, V.S.; Harish, B.M.; Jayanna, H.S.; Rajeeva, M.P.; Naveen, C.S.; Lamani, A.R. Synthesis, Characterization and Room Temperature Acetone Sensing of TiO₂ Nanotubes. *Sens. Lett.* **2018**, *16*, 105–109. [[CrossRef](#)]
85. Hazra, A.; Bhowmik, B.; Dutta, K.; Chattopadhyay, P.P.; Bhattacharyya, P. Stoichiometry, length, and wall thickness optimization of TiO₂ nanotube array for efficient alcohol sensing. *ACS Appl. Mater. Interfaces* **2015**, *7*, 9336–9348. [[CrossRef](#)] [[PubMed](#)]
86. Bian, H.; Ma, S.; Sun, A.; Xu, X.; Yang, G.; Gao, J.; Zhang, Z.; Zhu, H. Characterization and acetone gas sensing properties of electrospun TiO₂ nanorods. *Superlattices Microstruct.* **2015**, *81*, 107–113. [[CrossRef](#)]
87. Ramanavicius, S.; Tereshchenko, A.; Karpicz, R.; Ratautaite, V.; Bubniene, U.; Maneikis, A.; Jagminas, A.; Ramanavicius, A. TiO_{2-x}/TiO₂-Structure Based ‘Self-Heated’ Sensor for the Determination of Some Reducing Gases. *Sensors* **2020**, *20*, 74. [[CrossRef](#)]
88. Pandey, S.K.; Kim, K.H.; Tang, K.T. A review of sensor-based methods for monitoring hydrogen sulfide. *TrAC Trends Anal. Chem.* **2012**, *32*, 87–99. [[CrossRef](#)]
89. Moon, C.H.; Zhang, M.; Myung, N.V.; Haberer, E.D. Highly sensitive hydrogen sulfide (H₂S) gas sensors from viral-templated nanocrystalline gold nanowires. *Nanotechnology* **2014**, *25*, 135205. [[CrossRef](#)]
90. Carslaw, D.C.; Farren, N.J.; Vaughan, A.R.; Drysdale, W.S.; Young, S.; Lee, J.D. The diminishing importance of nitrogen dioxide emissions from road vehicle exhaust. *Atmos. Environ. X* **2019**, *1*, 100002. [[CrossRef](#)]
91. Predic, B.; Yan, Z.; Eberle, J.; Stojanovic, D.; Aberer, K. ExposureSense: Integrating daily activities with air quality using mobile participatory sensing. In Proceedings of the 2013 IEEE International Conference on Pervasive Computing and Communications Workshops, PerCom Workshops, San Diego, CA, USA, 18–22 March 2013; pp. 303–305.
92. Kaur, N.; Zappa, D.; Comini, E. Shelf Life Study of NiO Nanowire Sensors for NO₂ Detection. *Electron. Mater. Lett.* **2019**, *15*, 743–749. [[CrossRef](#)]
93. Engineer, C.B.; Hashimoto-Sugimoto, M.; Negi, J.; Israelsson-Nordström, M.; Azoulay-Shemer, T.; Rappel, W.J.; Iba, K.; Schroeder, J.I. CO₂ Sensing and CO₂ Regulation of Stomatal Conductance: Advances and Open Questions. *Trends Plant Sci.* **2016**, *21*, 16–30. [[CrossRef](#)]
94. Ponnuruvelu, D.V.; Pullithadathil, B.; Prasad, A.K.; Dhara, S.; Mohamed, K.; Tyagi, A.K.; Raj, B. Highly sensitive, atmospheric pressure operable sensor based on Au nanoclusters decorated TiO₂@Au heterojunction nanorods for trace level NO₂ gas detection. *J. Mater. Sci. Mater. Electron.* **2017**, *28*, 9738–9748. [[CrossRef](#)]
95. Wang, H.; Sun, Q.; Yao, Y.; Li, Y.; Wang, J.; Chen, L. A micro sensor based on TiO₂ nanorod arrays for the detection of oxygen at room temperature. *Ceram. Int.* **2016**, *42*, 8565–8571. [[CrossRef](#)]
96. Raza, M.H.; Kaur, N.; Comini, E.; Pinna, N. Toward Optimized Radial Modulation of the Space-Charge Region in One-Dimensional SnO₂-NiO Core-Shell Nanowires for Hydrogen Sensing. *ACS Appl. Mater. Interfaces* **2020**, *12*, 4594–4606. [[CrossRef](#)] [[PubMed](#)]
97. Fomekong, R.L.; Saruhan, B. Influence of humidity on NO₂-sensing and selectivity of spray-CVD grown ZnO thin film above 400 °C. *Chemosensors* **2019**, *7*, 42. [[CrossRef](#)]

